

NEAR-WAKE BEHAVIOR BEHIND TWO FLAT PLATES ARRANGED SIDE-BY-SIDE NORMAL TO FLOW***Ibrahim A. M. Gad[†]**

Faculty of Engineering, Zagazig University, Egypt.

ABSTRACT:

Two flat plates arranged side by side normal to air flow at high subcritical Reynolds number 20000 are investigated for near wake behavior by mean of three ways: 1) discrete vortex method (DVM) calculations, 2) smoke tunnel for near-wake visualizations and 3) wind tunnel for surface pressure measurements. FORTRAN computer language program is constructed for implementation of DVM calculations. Applying necessary refinements of some spectral techniques of DVM reduced the maximum differences between experimental and predicted results from 24.54% to 4.68%. The time variant and averaged aerodynamic forces, Strouhal number and near-wake configuration are investigated versus normalized time t and gap ratio (g/h) to understand the phenomena. The results agree satisfactory the previous literatures.

At $g/h \in (0.05:0.15)$ irregular mean drag observed, no biased gap flow pattern appears. The biased gap-flow pattern begin appears. At $g/h=0.2: 0.3$ the gap flow shows no any reattachment to the rear faces of plates occurred and the direction of the biasing remains the same unless some disturbance forms are introduced. The Coanda effect may be omitted from the principal causes of the biasing phenomenon. At $g/h \in (0.3:0.6)$ the gap flows appears always to be biased and flip-flops to the preferred side non-periodically with respect to time. At $g/h \in (0.6:1.25)$ the percentage of time occupied by the gap flow in the biased state decreases and the non-biased state of the gap flow becomes prevalent. At $g/h > 1.25$ the individual wakes of the plates behave independently. Generally the plate on the biased side showed high and regular vortex shedding, while those on the biased side showed the opposite.

KEYWORDS: Biased Gap Flow - side by Side – Two Flat Plate - Near-Wake

**PRES DE COMPORTEMENT SILLAGE DE DEUX PLATES PLAQUES
LATERALES DISPOSEES COTE A COTE NORMAL A L'ECOULEMENT
UNIFORME DE L'AIR****RÉSUMÉ**

Deux plaques planes disposées côte à côte normale au débit d'air à haute nombre de Reynolds sous critique 20000 sont d'une enquête pour comportement sillage proche de la moyenne de trois façons: 1) la méthode vortex discrète (DVM) calculs, 2) du tunnel de fumée pour les visualisations près-sommeil et 3) soufflerie pour les mesures de pression de surface. FORTRAN programme de langue ordinateur est construit pour la mise en œuvre des calculs DVM. Application des améliorations nécessaires de certaines techniques spectrales de la DVM réduit les différences maximale entre expérimental et les résultats prévus de 24,54% à 4,68%. La variante moyenne du temps et des forces aérodynamiques, nombre de Strouhal et configuration quasi-sommeil sont étudiées fonction du temps t normalisée et rapport de l'écart (g/h) pour comprendre les phénomènes. Les résultats sont en accord satisfaisant avec les littératures antérieures. Au $g/h \in (0.05:0.15)$ irrégulière glisser moyenne a été observée, aucune tendance écart biaisée débit apparaît. Le modèle biaisé écart-débit apparaît à commencer $g/h=0,2 :0,3$ montrant que l'effet Coanda peut être omise dans les principales causes du phénomène de polarisation, sans aucun rattachement à la face arrière est survenu et le sens de la polarisation reste le même sauf quelques formes de perturbation sont introduits. Au $g/h \in (0.3:0.6)$ l'écart des flux semble toujours d'être partielle et tongs pour le côté préféré non-périodique par rapport au temps. Au $g/h \in (0.6:1.25)$ le pourcentage de temps occupé par le flux dans le fossé diminue Etat partial et l'état non biaisée de la circulation écart devient courante. Au $g/h > 1,25$ sillages individuelle des plaques se comportent de façon indépendante. En général, la plaque sur le côté biaisé montré vortex haute et perte régulière, alors que ceux sur le côté biaisé a montré le contraire.

MOTS-CLES: le manque de débit écart - côte à côte - Deux plaques planes - proche sillage.

* Received: 12/12/2010, accepted: 22/1/2011 (original Paper)

† Contact author (iamg_51@yahoo.com)

1. INTRODUCTION

Physical insight into the biased gap flow occurring between two plates as phenomena of flow interaction, which may be useful in practical domains of aerodynamic forces and heat transfer, is needed. The published searches for investigation of biased gap flow behind two plates side by side are very few and insufficient in comparison with those for two circular or two rectangular cylinders. The first indication of the biased gap flow phenomena behind two circular cylinders arranged side by side to face the wind had been observed by Biermann and Herrstein (1933) but the causes of biasing was left without explain. Hori (1959) measured the surface pressure distribution around one of the two cylinders side by side at $Re = 8 \times 10^4$. He stated: For $g/h < 1.0$, there is a difference base pressure of the two cylinders. Ishigai, et al. (1972) photographed the flow pattern around the two cylinders and suggested that the biased gap flow was due to the Coanda effect, i.e., flow attaching itself more to one cylinder surface than the other due to unsymmetrical separation. Bearman and Wadcock (1973) measured the base pressure simultaneously on both cylinders, and found that the cylinders always experienced different base pressures in the range of spacing between $g/h = 0.1$ and 2.3 . The bi-stable nature of the biased flow pattern was confirmed. Zdravkovich (1977) concluded that for two circular cylinders arranged side by side the bi-stable gap flow represents a transition between the two staggered arrangements. Quadfflieg (1977)

insisted that the gap flow becomes a jet-like flow, so the Coanda effect causes the biasing. Kamemoto (1976), Kamemoto and Bearman (1980) and Stansby (1981) carried out theoretically modeling of separated shear layer by point vortex rows. Masanori et al. (1985) said after their experimental study that the turbulence which is characteristic of the high-Reynolds-number wakes may be omitted from the principal causes of the biasing phenomenon. They ensure that, once a biased gap-flow pattern appeared the direction of the biasing remains the same unless some disturbance forms are introduced. They added that this phenomenon is apparently different from the case of pair of circular cylinders, where the biased gap flow is not stable but changes direction abruptly at irregular intervals. They commented that the formation of shedding vortices on the unbiased side is considered to be the cause of the flip-flopping phenomenon observed. Arai et al., (1987) have been investigated numerically the flow around two rectangular cylinders arranged side by side by a discrete vortex method they said that steep interaction occurs at narrow gaps. Kim and Durbin (1988) and Behr et al. (1991) simulated the flow past two normal flat plates arranged side by side at low Reynolds numbers. They indicate that the direction of the biased flow was found to be switching at irregular intervals. Miao et al. (1996) studied flow over two side-by-side normal plates for which g/h are $0.4:1.1$ and $Re = 6.6 \times 10^3$ and 1.8×10^4 . At low g/h i.e., $0.4:0.6$ the gap flow appears always to be biased and flip-flops to

preferred side non-periodically with respect to time. As the g/h becomes larger, the percentage of time occupied by the gap flow in the biased state decreases and the non-biased state of the gap flow becomes prevalent. A comparison of the experimental results obtained under five free stream turbulence conditions further shows that the addition of artificial disturbance into the free stream promotes gap flow flopping at low g/h . Gad et al. (1999) had been investigated the two dimensional flow interference about two square prisms arranged side-by-side for different g/h at $Re=2 \times 10^4$ by DVM. They predicted the biased flow phenomenon and its instability. Wang et al. (2002) visualize the flow around two side-by-side circular cylinders and observed that an exceptionally large gap vortex occurred and subsequently triggered the changeover of the gap flow deflection from one side to another.

More quantitative aspects of the flopping phenomenon will require further study. This search attempts along this direction. The numerical analysis is conducted here by DVM. The DVM calculation can be divided into a main method and some complementary techniques (spectral techniques) (see Ref. (8 and 9)). In the present study, a FORTRAN computer language program is constructed for conducting the DVM calculations and refinement of its spectral techniques. Laboratory studies are conducted to guide the numerical experiments.

2. LABORATORY STUDIES

Laboratory studies are conducted to guide the numerical experiments. Flow visualizations are implemented by smoke tunnel. Surface pressure measurements are implemented by wind tunnels.

2. 1. Visualization of Flow

Smoke tunnel used in the present study is found in the hydraulic laboratory, Faculty of Engineering Zagazig University (see Ref. (9 and 10)). A visualization system has a unique advantage of variable slow-motion-playback, still framing, and slow motion reverse playback allowing a detailed and clear picture of the flow patterns is used. These variable motions are controlled manually by rotation of a specific switch by angle θ . The angle θ is proportional with the real flow time t_r . The working section is 180 mm wide, 240 mm height, and 100 mm deep. The thin plate models are fabricated from aluminum. All models are painted black. The plate model has 100 mm span, 10 mm in cord, and 1mm in thickness. The visualized cases are two flat plate models at different g/h .

2. 2. Pressure Measurements

The wind tunnel is of the open circuit type, it is found in the hydraulic laboratory, Faculty of Engineering Zagazig University (Ref. (9 and 10)). The working section (300mm x 75mm) has Perspex sides to give full

visibility, and the various multiple models are supported between the two sides. The flow patterns are two-dimensional and the maximum air velocity is nearly 45 m/sec. The empty tunnel was calibrated. No noticeable change than the calibration made by Gad et al. (1999) is found. The distribution over the full height of the working section is sensibly constant. The two flat plate models are fabricated with high accuracy from Perspex Fig 1.

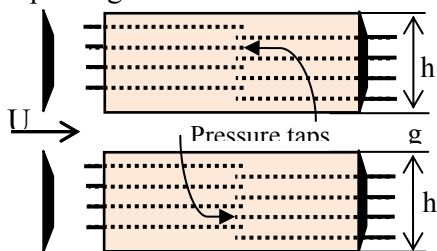


Fig. (1): Two plates model for surface pressure measurements

The plate cord is 30 mm with plate span equal 70 mm and thickness 3mm. The two plates are fabricated from Perspex and prepared with two span wise sharp edges. Each Perspex plate model is pierced longitudinally in the span wise direction of the plate by eight internal long holes reach to the mid span plan. Five pressure taps at front face and three at rear face are taken from the end of the eight holes. Each hole has a diameter of 0.5 mm and length equal half the span. The time averaged pressure is measured at the pressure taps. The time averaged drag forces, acting on the two bodies were estimated. The interference drag coefficient is calculated it is defined as: $C_{di} = C_{d1} - C_{d2}$ (1)

3. NUMERICAL INVESTIGATION (Discrete Vortex Method (DVM))

The detailed analysis of DVM can be found in Ref. (3, 7-10, 16, 20, 22, and 24). The DVM calculation can be divided into a main method and some complementary techniques (spectral techniques). The main DVM may be easily applied to any set of initial conditions, but have proven unreliable, resulting in chaotic motion of vortices after a finite time. The spectral techniques must be refined to give more reliable results but can be implemented efficiently only for special problems. The spectral techniques require the use of a number of non-disposable parameters usually unrelated to the conservation equations for the fluid.

3. 1. Main Method

3. 1. 1. Inviscid Model

The flow fields around two thin flat plates arranged side by side with gap ratios g/h in a uniform stream of velocity U normal to the plane of the two plates is treated. The Reynolds number is sufficiently large so that the flow can be simulated by an inviscid model with four thin separated and discredited shear layers. Each plate is replaced by number of bounded vortices. The surface singularity method is used for this purpose. The four separated shear layers at the four sharp edges of the two plates are replaced by a number of free discrete vortices in the following manner; After each time step Δt , four nascent

vortices are introduced at a distance h_4 away from its separation corner, see Fig. 2. At the start of each time step four nascent vortices are introduced at a distance h_4 away from its separation corner, see Fig. 2. The strength of s^{th} nascent vortex is given by:

$$\Gamma_{0s} = 1/2 V_{sh}^2 \Delta t \quad (2)$$

The shear-layer velocity V_{sh} (the velocity at the s^{th} separation edge) is taken equal the tangential velocity at the control point nearest to the s^{th} corner (at distance h_5 from the corner, see Fig 2). The position h_4 of nascent vortex must satisfy Kutta conditions (velocity = 0.0 at the edge). The second order - convection scheme is used for the convection of the free vortices in the wake.

3. 1. 2. Complex Potential:

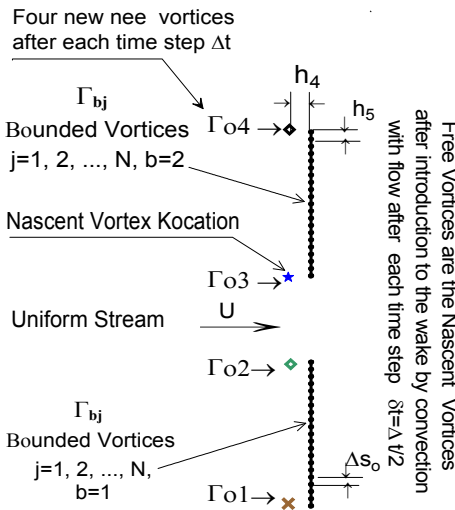


Fig. (2): Flow around two plate models prepared for numerical treatment as an inviscid model by modified DVM.

The complex potential describing the flow field is the superposition of:

- (a) Free stream ($-UZ$) (3)
- (b) Summation of bounded vortices located on the surfaces of two plates:

$$sum(\Gamma_{bj}) = \sum_{b=1}^2 \sum_{j=1}^N \Gamma_{bj} \quad (4)$$

- (c) Summation of wake vortices in the four shear layers emanated from the four nascent points near the four edges of the two plates:

$$sum(\Gamma_{bsn}) = \sum_{b=1}^2 \sum_{s=1}^4 \sum_{n=1}^{N_s} \Gamma_{bsn} \quad (5)$$

The complex potential is:

$$W(z) = -UZ + sum(\Gamma_{bj}) + sum(\Gamma_{bsn}) \quad (6)$$

$$\Gamma_{bj} = (1/2\pi) i\Gamma_{bj} \ln(Z - Z_{bbj}) \quad (7)$$

$$\Gamma_{bsn} = \frac{i\Gamma_{bsn}(-1)^\phi}{2\pi \ln(Z - Z_{bsn})} \quad (8)$$

$$-u + iv = -U + \sum_{b=1}^2 \sum_{j=1}^N \frac{i\Gamma_{bj}}{2\pi(Z - Z_{bj})} \quad (9)$$

$$+ \sum_{b=1}^2 \sum_{s=1}^4 \sum_{n=1}^{N_s} \frac{(-1)^\phi i\Gamma_{bsn}}{2\pi(Z - Z_{bsn})}$$

N is the number of bounded vortices distributed on each plate while N_s is the total number of vortices in the s^{th} shear layer. In equation 2; $\phi = 1$ and $\phi = 2$, for clockwise and anticlockwise vortex rotation, respectively.

3. 1. 3. Initial Conditions

Initially, at time $t=0$, the flow is assumed to be impulsively-started from rest. Then the time variation of

flow fields is computed at successive time steps Δt .

3. 1. 4. Boundary Conditions:

Zero normal velocity at the surfaces of the two solid plates is verified.

3. 1. 5. Computational Procedure:

The boundary condition generates a set of 2N simultaneous linear algebraic equations. The Gaussian elimination method is applied and the Kelvin theory is needed. The force components acting on each plate, F_x and F_y in U and its normal directions respectively, are computed by generalized unsteady Blasius theorem. The unsteady drag and lift coefficients for each plate are:

$$C_d = 2F_x/\rho h U^2 \quad (10)$$

$$C_l = 2F_y/\rho h U^2 \quad (11)$$

Time average force coefficients \bar{C}_l , \bar{C}_d and the Strouhal number, $S_t = fh/U$, for each plate have been calculated at the later stage of the motion where the transient behavior disappears. The Strouhal number is calculated from C_l curve as the inverse of the average time period, where f is the vortex shedding frequency.

3. 2. Spectral Techniques

3. 2. 1. Plate Presentation;

Two methods are tested here for the condition of zero normal velocity on the boundary; see (Ref. (11)). The first method verifies the zero internal tangential velocity, is used in [Smith](#) and Stansby (1988). The second method minimizes the error in normal

velocity at many control points as possible by the least square method Sarpakaya (1986).

3. 2. 2. Strength and Location of Nascent Vortices

The shear layer velocity V_{sh} is calculated at a distance h_5 from the corner (separated edge), along the wetted face.

The nascent vortex is introduced at a distance h_4 away from a corner. The nascent vortex strength (Ref. (15 and 22)) is:

$$\Gamma_0 = 0.5V_{sh}^2 \quad (12)$$

Kutta condition at this edge gives:

$$h_4 = V_{sh}\delta t/2\pi \quad (13)$$

Two convection schemes were tested for convection of the free vortices, for $\Delta t = 0.12$; A new vortex is introduced into the wake every Δt and all the calculations for convection are repeated every δt , where $\Delta t = 2\delta t$

3. 2. 3 Wake Vortices Convection

First order convection scheme is:

$$x(t + \Delta t) = x(t - \Delta t) + 2\Delta t u(t) \quad (14)$$

Second order convection scheme is:

$$x(t + \Delta t) = x(t) + 0.5[3u(t) - u(t - \Delta t)]\Delta t. \quad (15)$$

The second order scheme was preferred to minimize the error in convection process.

3. 2. 4. Vortex Decay

A simpler exponential decay law was tested. The vortex strength equal:

$$\Gamma = \Gamma_0 \text{EXP}(-\xi t^*), \quad (16)$$

ξ is a dissipation factor. This apparent vortex decay is then applied to every point vortex, based on its residence time in the flow. See Gad (2000). The core radius of a decaying line vortex which has been introduced in the wake of a viscous flow with $\text{Re}=4 \times 10^4$ is of the order of $0.025h$ see Robert (1997).

3. 2. 5. Shear Layer Velocity at Separation Corner

The shear layer velocity V_{sh} is calculated at a distance h_5 from the corner, along the wetted face.

3. 2. 6. Interaction among vortices themselves and with solid surface:

The present numerical experiments showed that it is more suitable to combine any two oppositely signed wake vortices when their separated distance less than or equal h_1 . For vortex, plate interaction, a vortex which approaches the plate surface within a specified distance h_2 is propagated parallel to the surface. Another method removes this vortex when approaching to the solid boundary (Ref. (27)).

4. RESULTS AND DISCUSSION

4. 1. Intervals Independent Solutions

The output results by refined DVM are expected to depend on the following arbitrary parameters: Δt , N , h_1^* , h_2^* , h_3^* , h_4^* , h_5^* ($h_5 = \Delta s_0$), ξ . The intervals independent numerical solutions of each of these parameters for limited maximum error will be searched. The aims are to obtain more reliable predicted results and stable

computations by defining the intervals of each parameter where the solution does not depend on the parameter itself. Many numerical experiments are needed for each of the above parameters separately when appearing in the calculations for first time. The value of the tested parameter is changed successively by small differences and the calculation of output variable is repeated after each change while the other parameters are retained constant. Three studied cases are undergone to this numerical analysis, 1) single plate, 2) two plates $g/h=0.1$ and 3) two plates 0.5 . Table 1, shows the tested interval for each parameter (column 1) and variation steps during the numerical tests (column 2). The results of analysis are presented in table 2 for error less than 5%; column 1 presents the intervals independent solution corresponding to each of the above arbitrary parameters while column 2 presents the chosen values of the parameters for the present paper. The results in table 2 show that the resulted intervals and chosen values may be the same for all studied cases.

Table (1): Numerical experiments

Tested interval	Variation step
$\Delta t \in [0.04 : 0.24]$	$\Delta t = 0.02$
$N \in [10 : 80]$	$\Delta N = 10$
$\xi \in [0.01 : 0.05]$	$\xi_5 = 0.05$
$h_1^* \in [0.01 : 0.05]$	$\Delta h_1^* = 0.005$
$h_2^* \in [0.01 : 0.05]$	$\Delta h_2^* = 0.005$
$h_3^* \in [0.01 : 0.05]$	$\Delta h_3^* = 0.005$
$h_4^* \in [0.01 : 0.05]$	$\Delta h_4^* = 0.005$
$h_5^* \in [0.01 : 0.05]$	$\Delta h_5^* = 0.005$

Table (2): Results of Numerical tests

Resulted Intervals	Chosen value
$\Delta t \in [0.04: 0.12]$	$\Delta t = 0.12$
$N \in [40: 80]$	$N = 40$
$\xi \in [0.02: 0.05]$	$\xi = 0.035$
$h_1^* \in [0.025: 0.035]$	$h_5^* = 0.035$
$h_2^* \in [0.025: 0.035]$	$h_5^* = 0.035$
$h_3^* \in [0.025: 0.035]$	$h_5^* = 0.035$
$h_4^* \in [0.025: 0.035]$	$h_5^* = 0.035$
$h_5^* \in [0.025: 0.035]$	$h_5^* = 0.035$

4. 2. DVM Validation

The predicted results in case of single flat plate by DVM for $h_1^*=h_2^*=0.07$ (outside their intervals of independent solution) and for $h_1^*=h_2^*=0.03$ (inside the intervals) are compared in Figs (a, b). It is clear that for all values of h_1^* and h_2^* lies outside their independent solution intervals the results are not smooth and suffer from high jitters.

4. 3. Measurements Uncertainty:

Important factor analysis is conducted based on measurement procedures and experience, in order to define the measurement function, that is, to determine the functional relationship between measured quantity Y and measurement quantity and factors that contribute to measurement uncertainty. This measurement function is employed to build uncertainty function. Then the uncertainty function is used to evaluate standard uncertainty values, which can be broken down into types A and B:

Type A is a way of statistical analysis on a series of observation values, in order to calculate standard uncertainty level. Its specific steps are as follows:

1. Repeat the test for n times
2. Obtaining the average X and standard deviation S

According to central limit theorem, the optimum standard deviation is acquired from the average after sampling from normal distribution.

Type B is a method of estimation using past measurement data, present understanding of devices or materials, specifications, calibration, or other figures provided by traceable certificate reports. Its steps of estimation are as follows:

1. Finding possible bias
2. Making an hypothesis about probability distribution
3. Calculating standard deviation according to hypothesized probability distribution

The standard deviation summation is achieved by communication theorem, multiplying type A and type B respectively by the weighting value endowed on importance of the measurement results, adding the respective products, find the square root of the total products, and acquiring the combination uncertainty value.

After the combination uncertainty value is obtained, in order to achieve a wider coverage, we multiply the value by the coverage factor K. Usually; we set the confidence coverage range to 95%, and expansion uncertainty U is acquired by multiplying the combination uncertainty value by K.

The final outcome of measurement:

$$Y = y \pm U.$$

The interference drag coefficient \bar{C}_{di} is the output of these measurements. To estimate \bar{C}_{di} an electronic manometer, thermometer, barometer and Pitot-static tub are used to measure $p - p_\infty$, t_∞ , p_∞ and $(P_t - P_\infty)$ respectively. A water manometer is used to calibrate the electronic manometer.

$C_d = D / (P_\infty U_\infty^2 / 2r T_\infty)$ D is calculated by pressure integration. The estimated value \bar{C}_{di} is influenced by the sensitivities of all the used instruments. Model and account for the sources of uncertainty that affect the final estimates \bar{C}_{di} uncertainty $U\bar{C}_{di}$ are built by the aid of (Ref. (8), and (28)). Monte Carlo simulation is employed to directly incorporate the combined uncertainties. A Gaussian probability distribution is assigned.

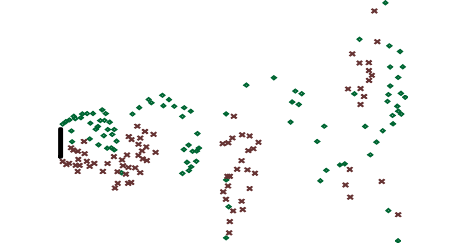
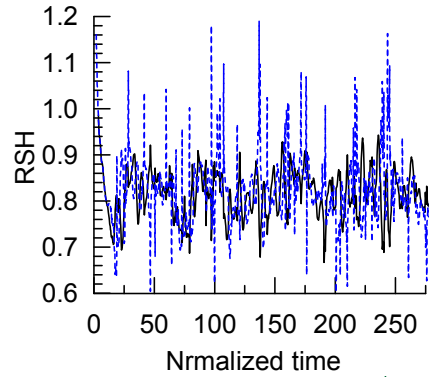
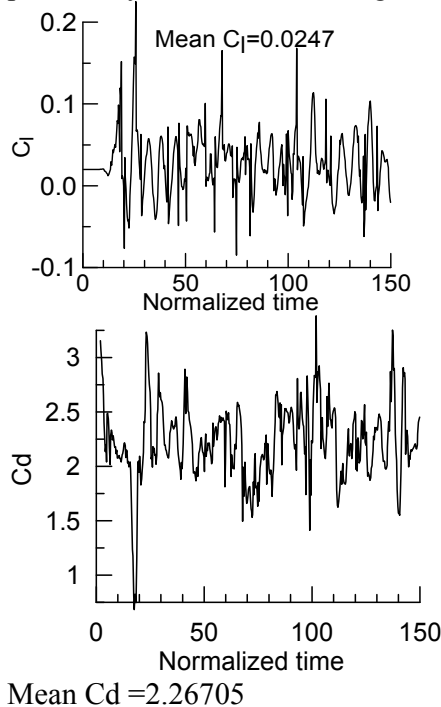
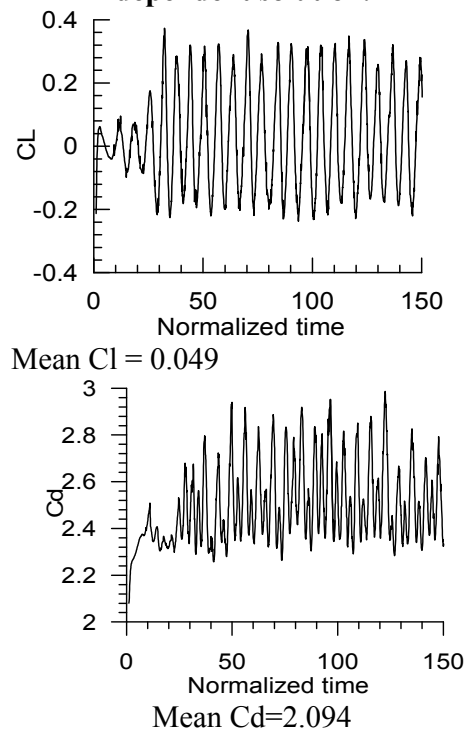


Fig. (4-a): Predicted characteristics of single flat plate $b/h=0.1$ by DVM, with $h_1=h_2=0.05h$ - outside intervals of independent solution.



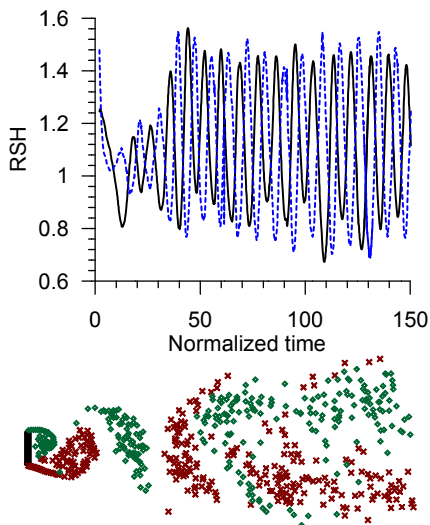


Fig. (4-b): Predicted characteristics of single flat plate $b/h=0.1$ by DVM with $h_1=h_2=0.03$ - inside the intervals of independent solution.

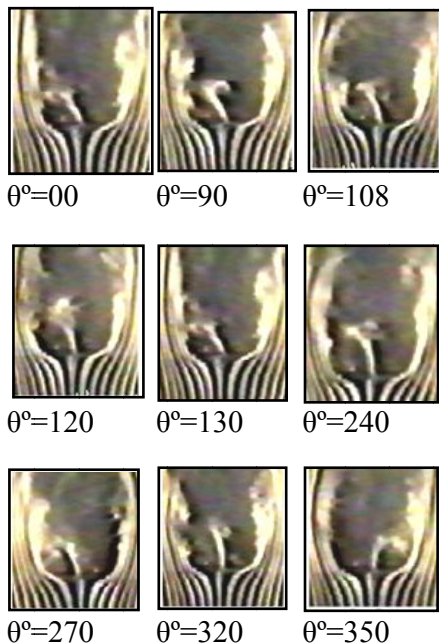
The calibration factor for electronic manometer was determined in a laboratory by fluid manometer. The local reference temperature during data collection is also needed. \bar{C}_{di} is generated with uncertainty $U\bar{C}_{di}=4.3\%$. Independent variables are treated at a level of confidence of 95%. This value of level of confidence is usually used.

4. 1. Smoke Tunnel Results Discussion

Two flat plates $g/h=0.3$ models $h=1\text{cm}$ and $b/h=0.1$ are visualized in the smoke tunnel for different g/h at $U_s=2\text{m/s}$ nearly. The behavior of the time variant near-wake flow was investigated by the visualization system mentioned above. Some species captured photos of visualized

gap flow for $g/h=0.3$ are presented in Fig 5. Each captured photo is marked by a value of θ , where θ is the angle of rotation of a switch (found in the visualization system) to be rotated for moving the video film in the moving video in the computer, θ is proportional with real flow time. For $g/h=0.3$ it is found that when films runs slowly the gap flow appears always to be biased to a preferred side non-periodically with respect to time. The cause of changing the direction of biased gap flow cannot be explained by this figure, only the phenomena can be red.

The visualization study of other gap ratios (not presented here - more than thousands photos are investigated in this study) shows that $\Delta\theta$ occupied by the gap flow in the biased state decreases by increasing the gab ratio. The biased state of the gap flow disappears for $g/h > 1.2$, Fig 6-a.



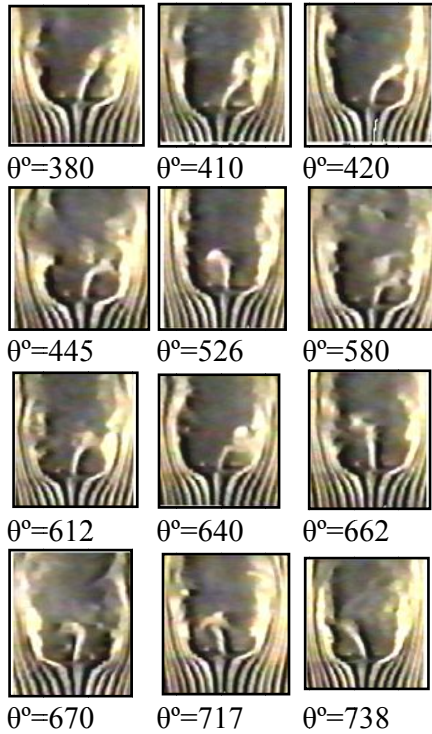


Fig. (5): Visualized time variant near wake behavior behind tow plates $g/h=0.3$, $U_s = 2m/s$ and θ^0 is proportional with real flow time t_r

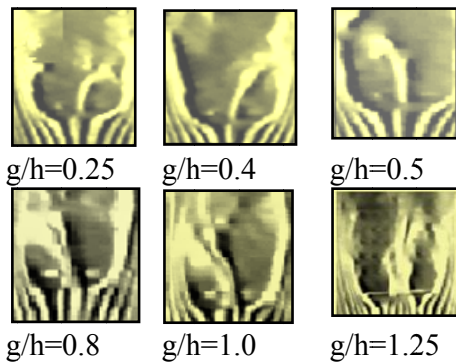


Fig. (6-a): Near-wake behavior vs. g/h

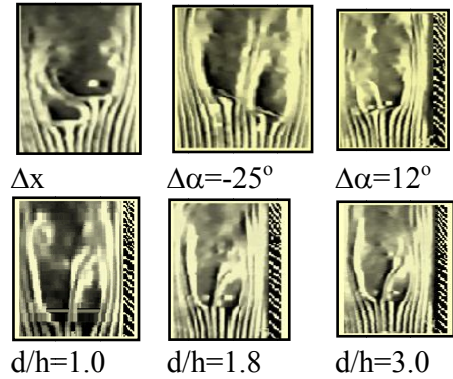


Fig. (6-b): Effects of asymmetric errors on the near-wake behavior $g/h=0.8$ for different d/h

Fig. (6-b) show that when the error Δx is posed by displacing one plate a small distance Δx in the flow direction, the gap flow is noticed to be biased toward the un-displaced plate. When errors $\Delta \alpha$ is posed by rotating the two plates together by small angle $\Delta \alpha$, the gap flow is found to be biased in the direction of the rotation of $\Delta \alpha$. Approaching one outer edge of the two plates near a solid wall; it is noticed that the gap flow is biased toward the wall. These simple tests led to conclusion that the gap flow behavior may be depend on the flow field and the solid boundary surrounding the gap flow only.

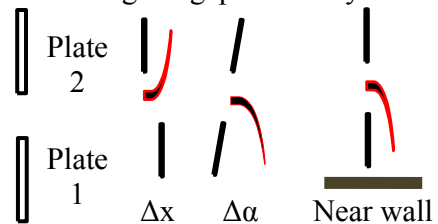


Fig. (7): Sketch of the effect of some errors in the two plates positions on the biased gap flow direction

The time average drag coefficients acting on the two plates for different gap ratios g/h are predicted by DVM and presented in Fig 8-a. This figure shows that the two time-averaged drag coefficients \bar{C}_{d1} and \bar{C}_{d2} acting on the two plates for $g/h > 2.5$ are equal. This may be meant that the biased flow phenomena disappeared for $g/h > 2.5$.

For the interval $0.7 < g/h < 2.5$ \bar{C}_{d2} is always greater than \bar{C}_{d1} . This may be meant that the biased gap flow is toward plate 2 in preferred direction or in stable condition for $0.7 < g/h < 2.5$. For $0.2 < g/h < 0.7$ the sign of the difference between \bar{C}_{d1} and \bar{C}_{d2} is noticed to be changed.

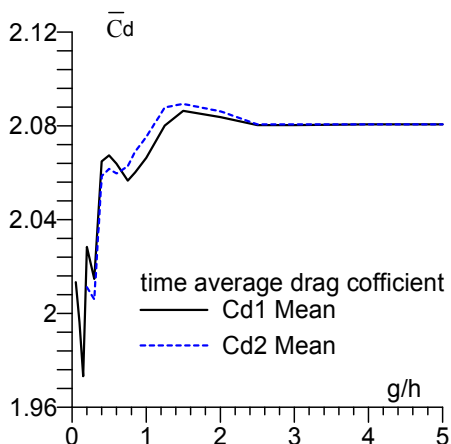


Fig. (8-a): Predicted time average drags coefficients acting on the two plates for different gap ratios g/h .

This may be due to the changing the preferred biased flow direction for $0.2 < g/h < 0.7$. For $g/h < 0.15$ the figure shows that the DVM failed to simulate this type flow.

Figure 8-b presents the predicted and experimental interference mean

drag coefficient \bar{C}_{di} acting on the two plates $b/h=0.1$ for $0.05 < g/h < 5.0$. The figure shows reasonable agreement between the predicted and the experimental results for $g/h > 0.2$ while for $g/h < 0.2$ the comparison shows non logic differences. This may be explained by the failure of DVM to simulate this flow for very narrow gaps $g/h < 0.2$ due to the complexity of convection process of shedding vortices from the two edges 2 and 3.

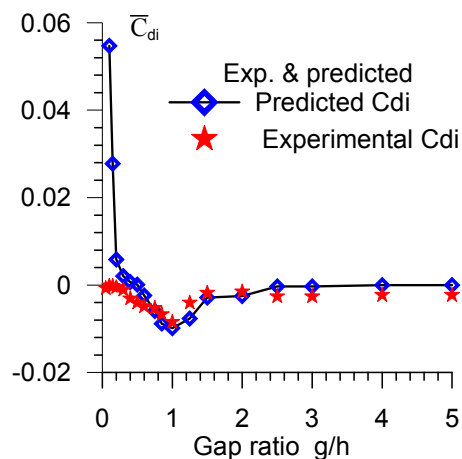


Fig. (8-b): predicted and experimental interference mean drag coefficients acting on the two plates for different gap ratios

Instantaneous pressure coefficient distributed over the surface of the two plates having gap ratio $g/h=0.75$ is predicted by refined DVM at two chosen instants. Fig 9-a presents a case of strong gap flow deflection toward the upper plate at normalized time $t = 33.12$. The figure shows identical instantaneous pressure coefficient distribution C_p at the front faces of the two plates., while at the rear faces the

base pressure coefficient C_{pb} at the plate in biased direction (upper plate) has a lower value than the other plate with high difference, this mean that the drag coefficient acting on upper plate is greater than that of lower plate. Fig 9-b presents a case of weak gap flow deflection toward the lower plate at normalized time $t = 69.44$. The figure shows also that the pressure distribution at the front faces are identical, while at the rear faces the base pressure coefficient at the upper plate and lower plate have low differences. Therefore the discrete vortex method DVM and its refined spectral techniques predict that the plate on the biased side has a lower instantaneous base pressure (or higher instantaneous drag) than those on the plate on unbiased side.

The predicted time variant near wake behavior by DVM is presented in Fig 10-a. This figure shows that the gap flow is biased toward upper or lower plate in a similar manner shown in visualized flow in smoke tunnel Fig 5. The plate on the biased side showed more regular vortex shedding than the other.

The near-wake configuration for different gap ratio at normalized time equal 300 nearly is predicted by DVM. The studied gap ratios by DVM are $g/h = 0.05, 0.1, 0.15, 0.2, 0.25, 0.3, 0.4, 0.5, 0.6, 0.7, 0.75, 0.85, 1.0, 1.25, 1.5$ and 2.5 . A FORTRAN program is constructed in the present search for this purpose. The results are presented in Fig 10-b. It is noticed that; for the three studied cases $g/h = (0.05, 0.1$ and $0.15)$ the two outer shear layers 1 and 4 behave like its behavior in case of a

single plate of height $2h$. While the two gaps shear layers 2 and 3 seem to be leaked in two air weak steams from the narrows gaps crossing each other without any reattaching the rear walls of the two plates. The two gap shear layers, leaks making an angle $10^\circ: 25^\circ$ nearly with the other plate. The Coanda effect doesn't exist here. In $g/h = 0.15$ the two gap shear layers begin to be mixed behind the two plate wall. In $g/h = 0.2, 0.25$ and 0.3 the two gap shear layers exit from the gap in two straight surfaces parallel to each other deviated by angle toward one plate in stable manner. For $g/h = 0.05: 0.15$ the majority gap vortices 2 and 3 are expected to be consumed by combination process. The few resulted number of vortices are spread and distributed in random way in the clusters formed by 1 and 4 to maintain their asymptotic equilibrium. For $g/h = 0.05: 0.25$ the configuration of the near wake seems to be in stable condition. For $g/h = 0.3 < g/h < 1.25$ the gap flow biased in a curved manner toward one plate; if any gap ratio is studied for time variant near-wake behavior it is noticed that the flip flop phenomena is appeared Fig 10-a. For $g/h > 1.25$ the biasing flow is switched.

The case of single plates having $b/h = 0.1$ and $h = 3\text{cm}$ is studied numerically and experimentally for DVM validation. One plate (Fig 1) placed normally to uniform air stream of average speed 9.687 m/s have been investigated in the two-dimensional wind tunnel where the estimated density $\rho = 1.215\text{ kg/m}^3$. The mean pressure distributions on the two faces (front and back) are measured and the

mean drag coefficient \bar{C}_{ds} is estimated. It is found that $\bar{C}_{ds} = 1.98$ in this case. The measurements of surface pressure are repeated in cases of two plates for different g/h and the time averaged values of \bar{C}_{d1} , \bar{C}_{d2} and \bar{C}_{di} are estimated from equation 1.

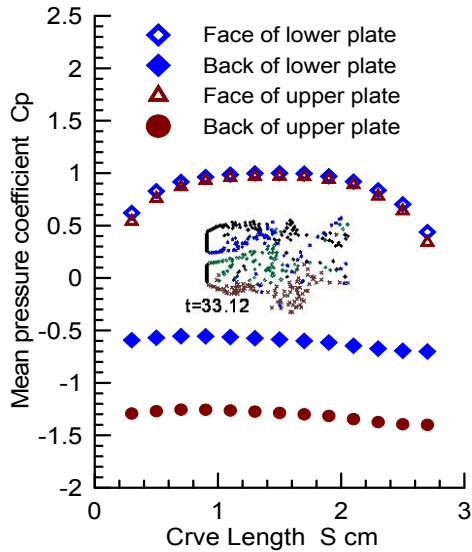


Fig. (9-a): Case of strong upward gap flow deflection – the base pressure coefficient is lower behind the plate in the deflection side.

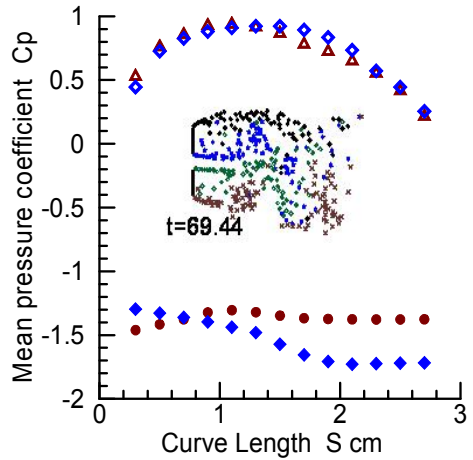
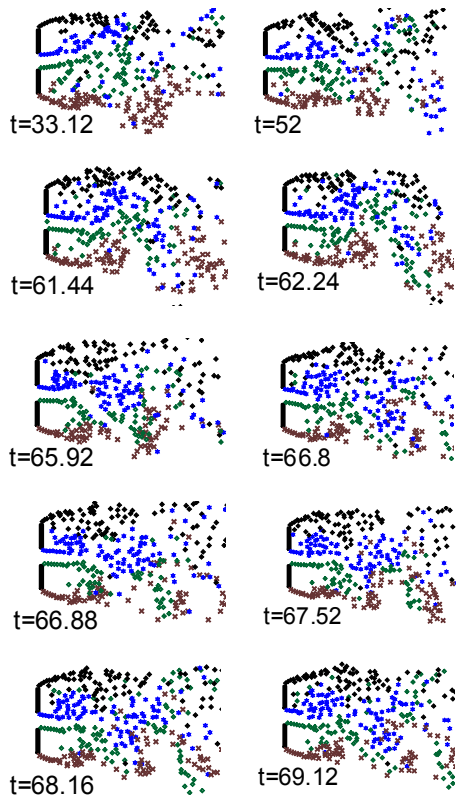


Fig. (9 – b): weak downward gap flow deflection – the differences between the two base pressure coefficients are



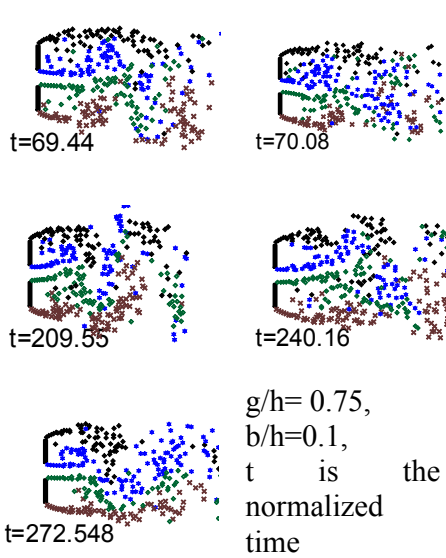


Fig. (10-a): DVM prediction of time variant near-wake behavior behind the two plates, $g/h = 0.75$

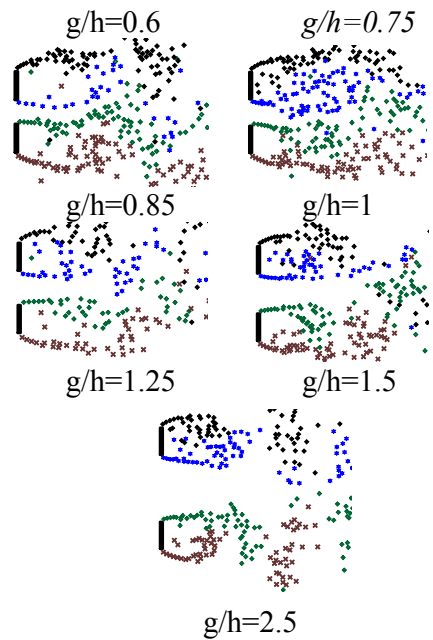
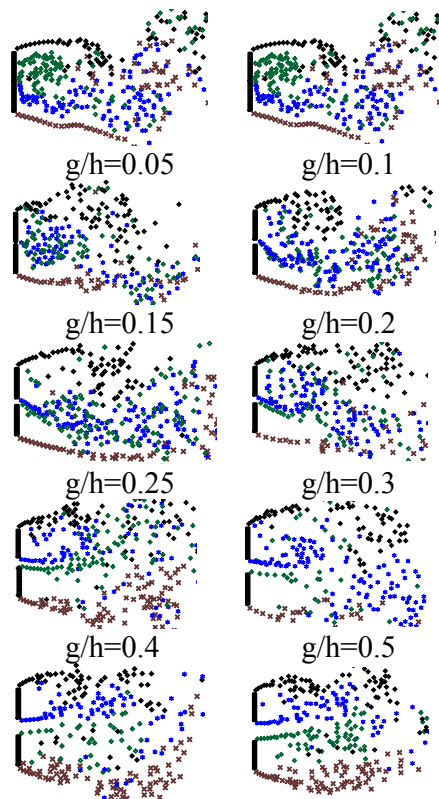
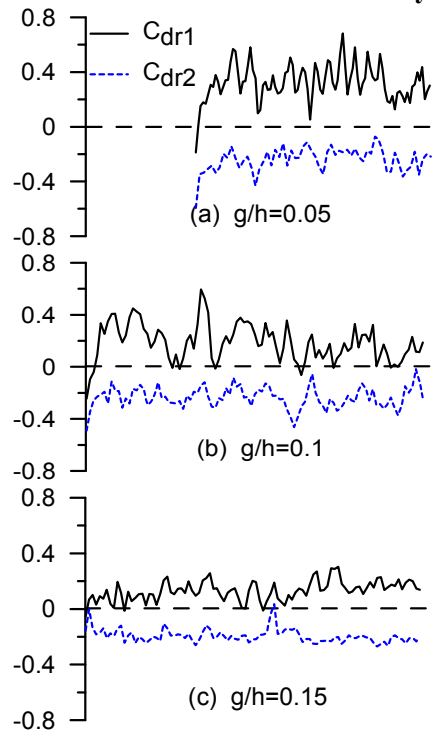


Fig. (10-b): DVM prediction of near-wake behavior for different gap ratio at normalized time $t=300$ nearly



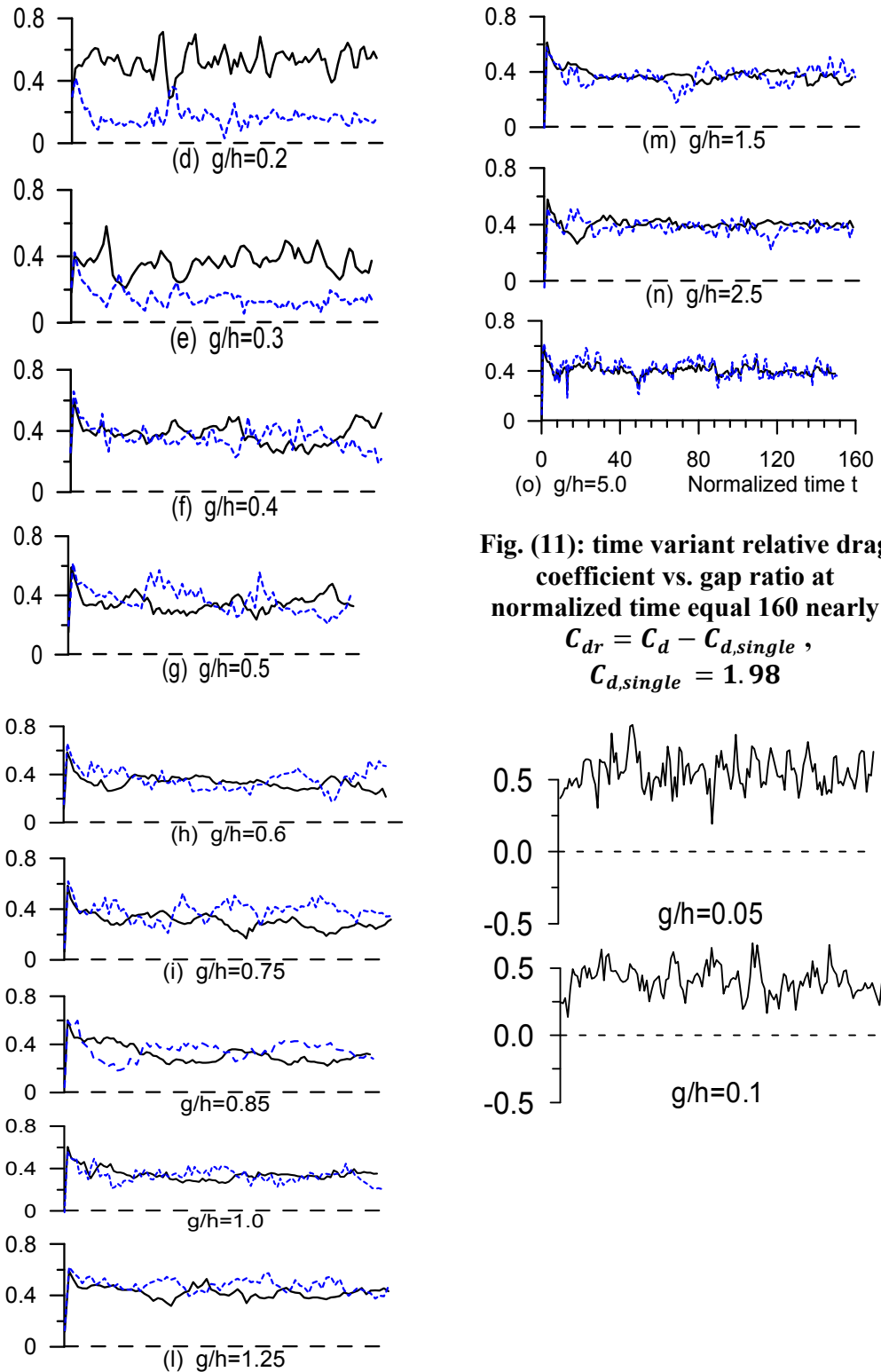
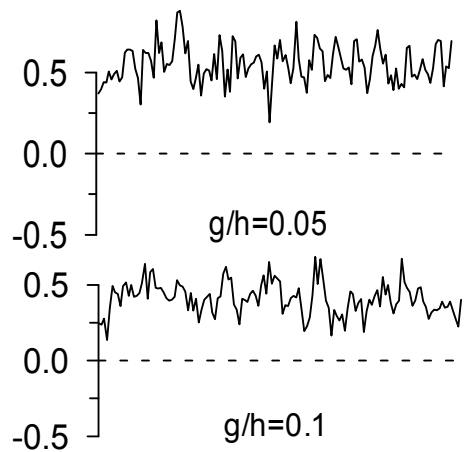


Fig. (11): time variant relative drag coefficient vs. gap ratio at normalized time equal 160 nearly

$$C_{dr} = C_d - C_{d,single} ,$$

$$C_{d,single} = 1.98$$



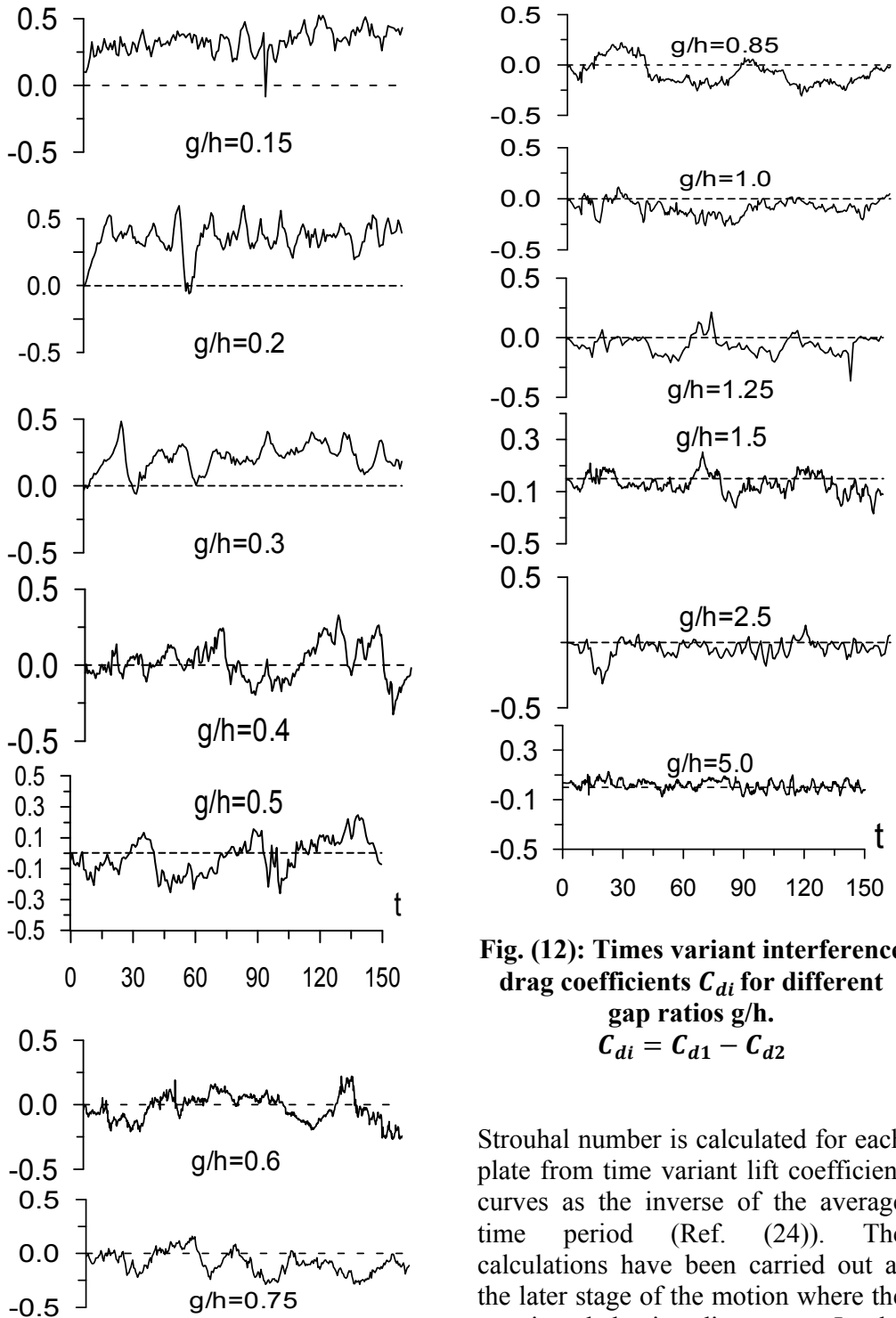


Fig. (12): Times variant interference drag coefficients C_{di} for different gap ratios g/h .

$$C_{di} = C_{d1} - C_{d2}$$

Strouhal number is calculated for each plate from time variant lift coefficient curves as the inverse of the average time period (Ref. (24)). The calculations have been carried out at the later stage of the motion where the transient behavior disappears. In the range of the present study the drag

coefficients as well as the Strouhal number are independent of Reynolds number (Ref. (1) and (13)). These remarks may explain the validity of comparison the visualization results at $Re = 2.3 \times 10^3$ with the numerical and experimental results at $Re = Uh/\nu = 2 \times 10^4$.

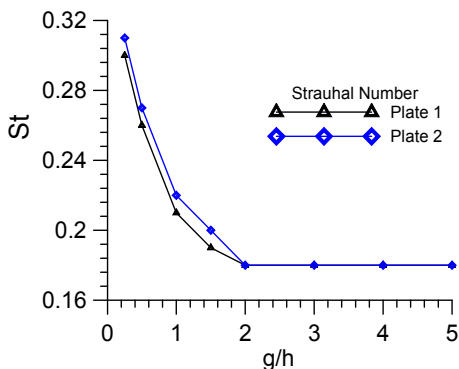


Fig. (13): Predicted Strouhal number for the two plates versus gap ratios, $S_t = fh/U$

5. CONCOLUSIONS

Single cusped edges flat plate having $b/h=0.1$ and $h=3\text{cm}$ placed normal to a uniform incompressible air stream is experimentally tested in wind tunnel and numerically by inviscid refined DVM. The primary aim is to validate the DVM and its spectral techniques refining the method. The original aim of the search is to investigate near-wake behavior behind two flat plates arranged side-by-side normal to flow.

The intervals, satisfying parameter independent solution, are determined by repeated numerical tests see table 1.

These intervals are then used to investigate two flat plates arranged side by side normal to air flow at $Re = 20000$ for near wake behavior at different g/h and various normalized time t . Smoke tunnel for near-wake visualizations and wind tunnel for surface pressure measurements are used for the two plates investigations. FORTRAN computer program is constructed for DVM calculations.

The refinements of DVM spectral techniques reduced the maximum differences between experimental and predicted results from 24.54% to 4.68%, so the results obtained agree satisfactory the previous literatures and the present experiment as well as the visualized near wake patterns.

Depending on various gap ratios and normalized time the gap flow can be categorized as follow:

- 1) At $g/h \in (0.05:0.15)$ irregular mean drag observed, no biased gap flow pattern appears, the Coanda effect may be omitted from the principal causes of the biasing phenomenon.
- 2) Once a biased gap-flow pattern appears at $g/h = 0.2$ and 0.25 , the direction of the biasing remains the same unless some disturbance forms are given.
- 3) At $g/h \in (0.3:0.6)$ the gap flows appears always to be biased and flip-flops to the preferred side non-periodically with respect to time.
- 4) At $g/h = (0.6:1.25)$ the percentage of time occupied by the gap flow in the biased state decreases and the non-

biased state of the gap flow becomes prevalent.

5) At $g/h > 1.25$ the individual wakes of the plates behave independently.

6) Generally the plate on the biased side showed high and regular vortex shedding, while those on the biased side showed the opposite.

7) Biased gap flow and Coanda effect are two different phenomena, each one need other catalyst come from the surrounding flow fields created by the solid boundary.

ACKNOWLEDGEMENT:

Many thanks for Prof. Dr. Mohammed Raafat Shaalan, who gave the opportunity to publish this paper and for his useful advices during this research.

REFERENCES

- 1-Achenbach E., (1975), "Total and Local Heat Transfer from a Smooth Circular / in Cross-Flow at High Reynolds Number", Int. J. Heat Mass Transfer, Vol. 18, pp. 1387-1396.
- 2-Arai N., Taguchi K., and Tani T., (1987) "Numerical Investigation of Flow around two rectangular cylinders by a Discrete Vortex Method" Nippon Kikai Gakkai Ronbunshu, B hen Vol. 53 No 486, pp 363-370.
- 3-Aso, S., and Hayashi, M., (1990), "Numerical Simulation of Separated

Flows around Bluff Bodies by Discrete Vortex Method", Memoirs of the Faculty of Eng., Kyushu Univ., Vol. 50, No 3.

- 4-Bearman, P. W., and Wadcock, A. J., (1973), "The interaction between a pair of Circular Cylinders Normal to a stream", Journal of Fluid Mechanics, Vol. 61, pp. 499-511.
- 5-Behr, M., and Tezduyar, T.E., (1991), "Wake Interference Behind Two Flat Plate Normal to the Flow: A Finite Element Study", Theoretical and Computational Fluid Dynamics 2, pp 223-250.
- 6-Biermann, D., and Herrnstein, W. H., Jr., (1933), "The interference between Struts in Various Combinations", National Advisory committee for Aeronautics, Tech. Rep. 486.
- 7-Bienkiewicz, B., and Kutz, R. F., (1990), "Applying the Discrete Vortex Method to Flow about Bluff Bodies" J. of Wind Eng. and Industrial Aero, Vol. 36, pp 1011-1020.
- 8-Coleman, H. W. and Steele, W. G., (1989), "Experimentation and Uncertainty for Engineers", New York: J. Wiley.
- 9-Gad, I. A., El-Taher, R. M., and Atia, R. M., (1999), "Characteristics of Flow Interaction around Two Square Prisms Arranged Side-by-Side", Alexandria Eng., Journal Vol. 38 No. 4, A195-A211 Faculty

- of Eng., Alexandria University - Egypt July M. vortex streets”, Bull. JSME 19, 283–290.
- 10-Gad, I. A., (2000), “Refined Model of Discrete Vortex Method Applied to Sharp Edged Bodies”, Journal of Engineering and Applied Sciences, Faculty of Engineering, Cairo University, V. 48-3.
- 11-Graham, J. M. R., (1986), “Application of The DVM to The Computation of Separated Flows” J. Numerical Methods for Fluid Dynamics II Clardon Press, Oxf., Vol. 7, pp 273-302.
- 12-Hori, E., (1959), “Experiments on flow around a pair of Parallel Circular Cylinders”, Proceedings, 9th Japan National Congress for Applied Mech., Tokyo, Japan.
- 13-Igarashi, T., (1987), “Fluid Flow and Heat Transfer around Rectangular Prisms (The Case of a Width/Height ratio of a section of 0.33: 1.5)”, Int. J. Heat Mass Transfer, Vol. 30, No. 5, pp. 893-901.
- 14-Ishigai, S., Nishikawa, E., Nishikmura, K., and Cho, K., (1972), “Experimental study on structure of gas flow in Tube Banks with Tube Axes normal to flow (Part 1, Karman Vortex flow around two Tubes at Various Spacing)”, Bulletin of the Japan Society Mechanical Engineers, Vol. 15, No. 86, pp. 949-956.
- 15-Kamemoto, K., (1976), “Formation and interaction of two parallel vortex streets”, Bull. JSME 19, 283–290.
- 16-Kamemoto. K. and Bearman, P. W., (1980), “An inviscid model of interactive vortex-shedding behind a pair of flat plates arranged side by side to approaching flow”, Trans. JSME 46., pp. 1220-1236.
- 17-Kelkar, K. M. and Patankar, S., (1992) “Numerical Prediction of Vortex Shedding behind a Square Cylinder”, International Journal for Numerical Methods in Fluids, Vol. 14, pp 327-341.
- 18-Kim, H. J., and Durbin, P.A., (1988), "Investigation of the flow between a pair of circular cylinders in the flopping regime", Journal of Fluid Mechanics 196, pp 431–448.
- 19-Masanori, H., Sakurai, A., and Ohya, Y., (1986), “Wake interference of a row of normal flat plates arranged side by side in a uniform flow”, Journal of Fluid Mechanics 164:1-25, Cambridge University Press.
- 20-Miau, J.J., Wang, H.B., and Chou, J.H., (1996), “Flopping phenomenon of flow behind two plates placed side-by-side normal to the flow direction”, Fluid Dynamics Research, 17, pp 311-328.
- 21-Okajima, A., (1990), “Numerical Simulation around rectangular cylinders”, Journal of Wind Engineering and Industrial Aerodynamics, Vol. 33, pp 1011-1020.

- 22-Quadfflieg, H., (1977), "Vortex induced load on the cylinder pair at high Reynolds number", (in German) *Forsch. Ing. Wes.*, vol. 43, pp.9-18.
- 23-Robert, R. H., and Chia, C. Y., (1997), "A Numerical Study of Vortex Shedding from a Square Cylinder with Ground Effect", *ASME Journal of Fluid Engineering*, Vol.119, pp 512-518.
- 24-Sarpkaya, T., and Ihrig, C.J., (1986), "Impulsively Started Flow about Rectangular Prisms: Experimental and Discrete Vortex Analysis" *J. Fluids Eng.*, 108, pp 47-54.
- 25-Sarpkaya, T., (1994), "Vortex Element Method for Flow Simulation", *Advances in Applied Mechanics*, Vol. 31, pp 113-247.
- 26-Smith, P.A. and Stansby, P.K., 1988. Impulsively started flow around a circular cylinder by the vortex method. *Journal of Fluid Mechanics* **194**, pp. 45–77.
- 27-Stansby, P. K., (1981), "A numerical study of vortex shedding from one and two circular cylinders", *Aero Q.* 32, 84-71.
- 28-Steele, W.G., Ferguson, R.A., Taylor, R.P., Coleman, H.W., (1994), "Comparison of ANSI/ASME and ISO models for calculation of uncertainty", Volume 33, Issue 4, 339-352.
- 29-Wang, Z., Zhou, Y., and Hui, L., (2002), "Flow-Visualization of A Two Side-By-Side Cylinder Wake", *Journal of Flow Visualization and Image Processing*, Vol. 9 Issue 2&3.
- 30-Zdravkovich, M. M., (1977), "Review of Flow Interaction between Two Circular Cylinders in Various Arrangements", *Trans. ASME I. J. Fluid Eng.* 99, pp 618-632.

NOMENCLATURE:

b	Plate thickness
C_d	Time variant drag coefficient
C_l	Time variant lift coefficient
\bar{C}_d	Time averaged drag coefficient
\bar{C}_{ds}	Drag coefficient – single plate
C_{dr}	$C_{dr} = C_d - \bar{C}_{ds}$
C_{di}	$C_{di} = C_{d1} - C_{d2}$
d	nearest distance between the plate edge and the near wall
f	vortex shedding frequency
g	Gab between the two plates
h	plate height
h_1	separation distances used for coalescence
h_2	separation distances for removal techniques
h_3	constant vortex radius for decaying
h_4	distance from corner to the point of calculated V_{sh}
h_5	distance away from a corner
N	number of Bounded Vortices for one plate

N_s	total Number of free Vortices in a Shear Layer s, $N_s = t/\Delta t$
Re	Reynolds Number
s	Number of Shear Layer
St	Strouhal Number
t	Normalized Time $t_r \cdot U/h$
t^*	vortex age
t_r	real time
T	periodic time
U	Free Stream Velocity
V_{sh}	shear layer velocity
F_x	Force component acting on each plate in uniform stream direction
F_y	Force component acting on each plate normal to uniform stream direction

Abbreviations

DVM	Discrete vortex method
FV1	Free vortices emanated from outer edge of plate 1
FV2	Free vortices emanated from gap edge of plate 1
FV3	Free vortices emanated from gap edge of plate 2
FV4	Free vortices emanated from outer edge of plate 2

Greek Symbols

α	Incidence angle equal zero in the present study
Γ	Vortex Strength
ξ	dissipation parameter